Soft Matter

PAPER

View Article Online
View Journal | View Issue

Cite this: *Soft Matter*, 2020, **16**, 983

Structure and dynamics of lipid membranes interacting with antivirulence end-phosphorylated polyethylene glycol block copolymers†‡

Jing Yu, §[ab] Jun Mao,[ab] Michihiro Nagao, [cd] Wei Bu, [e] Binhua Lin, [ef] Kunlun Hong, [g] Zhang Jiang,[h] Yun Liu,[ci] Shuo Qian, [j] Matthew Tirrell *[ab] and Wei Chen *[ab]

Received 13th August 2019,
Accepted 6th December 2019

DOI: 10.1039/c9sm01642b

rsc.li/soft-matter-journal

The structure and dynamics of lipid membranes in the presence of extracellular macromolecules are critical for cell membrane functions and many pharmaceutical applications. The pathogen virulence-suppressing end-phosphorylated polyethylene glycol (PEG) triblock copolymer (**Pi-ABAPEG**) markedly changes the interactions with lipid vesicle membranes and prevents PEG-induced vesicle phase separation in contrast to the unphosphorylated copolymer (**ABAPEG**). **Pi-ABAPEG** weakly absorbs on the surface of lipid vesicle membranes and slightly changes the structure of 1,2-dimyristoyl-*sn*-*glycero*-3-phosphocholine (**DMPC**) unilamellar vesicles at 37 °C, as evidenced by small angle neutron scattering. X-ray reflectivity measurements confirm the weak adsorption of **Pi-ABAPEG** on **DMPC** monolayer, resulting in a more compact **DMPC** monolayer structure. Neutron spin-echo results show that the adsorption of **Pi-ABAPEG** on **DMPC** vesicle membranes increases the membrane bending modulus κ.

Introduction

Polyethylene glycol (PEG) is widely applied in PEG-conjugated ("PEGylated") pharmaceuticals for protein/peptide conjugation.[1] A recent discovery by our group showed that an end-phosphorylated PEG copolymer with a hydrophobic bisphenol A (BPA) centre (**Pi-ABAPEG**) could be used as the virulence-directed agent for treating diseases and disorders involving microbial pathogens, such as intestinal microbial pathogens, *e.g.*, Pseudomonas aeruginosa.[2–4] Those diseases and disorders characterized by an epithelium attacked by a microbial pathogen are contemplated, including gastrointestinal infections and inflammation, *e.g.*, treatment of intestinal or oesophageal anastomosis or treatment or suppression of anastomotic leakage. **Pi-ABAPEG** (Fig. 1) integrates the effect of inorganic phosphate, a key and universal "cue" in response to which bacteria either enhance their virulence when local phosphate is scarce or downregulate it when phosphate is abundant, at the end of both PEG polymer blocks, resulting in effective inhibition of the multidirectional signalling between microbes, pathogens, and the host response.[2–4] *In vivo* studies show that the unphosphorylated **ABAPEG** copolymer strongly interacts with epithelial membrane lipid rafts, key structures involved in cell signalling transduction, preventing dysregulation of barrier function and apoptosis.[4,5] To understand the protective effect of **Pi-ABAPEG** better, a clear understanding of how PEGylated polymers affect the structure and dynamics of phospholipid membranes is necessary.[4,6,7]

[a] *Centre for Molecular Engineering and Materials Science Division, Argonne National Laboratory, Lemont, IL, 60439, USA. E-mail: wchen@anl.gov*
[b] *Pritzker School of Molecular Engineering, University of Chicago, Chicago, IL, 60637, USA. E-mail: mtirrell@uchicago.edu*
[c] *NIST Centre for Neutron Research, National Institute of Standards and Technology, Gaithersburg, MD, 20899-6102, USA*
[d] *Centre for Exploration of Energy and Matter, Indiana University, Bloomington, IN, 47408, USA*
[e] *Centre for Advanced Radiation Sources, University of Chicago, Chicago, IL, 60637, USA*
[f] *James Franck Institute, University of Chicago, Chicago, IL, 60637, USA*
[g] *Centre for Nanophase Materials Sciences, Oak Ridge National Laboratory, Oak Ridge, TN, 37831, USA*
[h] *Advanced Photon Source, Argonne National Laboratory, Lemont, IL, 60439, USA*
[i] *Department of Chemical and Biomolecular Engineering, Centre for Neutron Science, University of Delaware, Newark, DE, 19716, USA*
[j] *Biology and Soft Matter Division, Oak Ridge National Laboratory, Oak Ridge, TN, 37831, USA*

† Certain commercial materials are identified in this paper to foster understanding. Such identification does not imply recommendation or endorsement by the National Institute of Standards and Technology, nor does it imply that the materials identified are necessarily the best available for the purpose.

‡ Electronic supplementary information (ESI) available: Contrast matching and SLD determination of hPi-ABAPEG and dPi-ABAPEG, SANS profiles and NSE spectra of **ABAPEG** and **Pi-ABAPEG**, and X-ray reflectivity of **DMPC** monolayers at the air–water interface. See DOI: 10.1039/c9sm01642b

§ Current address: School of Materials Science and Engineering, Nanyang Technological University, Singapore, 639798, Singapore.

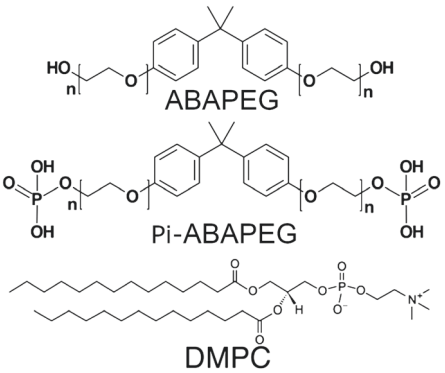

Fig. 1 The chemical structures of **ABAPEG**, **Pi-ABAPEG**, and **DMPC**.

Phospholipid bilayers recapitulate many features of living cell membranes: they are highly flexible, self-assembled, supramolecular structures that can undergo different dynamic conformational transitions.[8] This flexibility of membrane structure is key to many biological processes, including cell adhesion, cellular uptake and release, and cellular signalling events.[9–11] A variety of techniques, including fluctuation spectroscopy,[12,13] micropipette aspiration,[14] electro-deformation,[15] atomic force microscope (AFM),[16] optical tweezers,[17] X-ray scattering,[18,19] and neutron spin echo spectroscopy,[20] have been employed to study the membrane elastic properties. The extracellular environment also affects the structure and function of lipid membranes.[21] Proteins, polysaccharides, proteoglycans, and various synthetic polymers can insert into or adsorb on the membrane surface, which alter membrane structure and dynamics and, thereby, affect membrane functionalities.[22–24] The investigation of membrane structure and dynamics in the presence of extracellular macromolecules has drawn great attentions.[21,25–28]

In this paper, we report the experimentally measured structure and elasticity of 1,2-dimyristoyl-*sn-glycero*-3-phosphocholine (**DMPC**) model membrane in the presence of **Pi-ABAPEG** (Fig. 1). The thermal fluctuation and undulation of **DMPC** unilamellar vesicle (ULV) membranes were measured using neutron spin-echo spectroscopy (NSE) complemented with structural characterization using dynamic light scattering (DLS), small angle neutron scattering (SANS) and X-ray reflectivity (XRR) techniques.

Experimental methods

Synthesis and characterization of ABAPEG and Pi-ABAPEG

The **ABAPEG** triblock copolymers contain a hydrophobic BPA centre and two short PEG ($\approx$5 K) segments. Both protonated and deuterated **ABAPEG** triblock copolymers (hABAPEG and dABAPEG) were synthesized through anionic ring-opening polymerization of protonated and deuterated ethylene oxide (hEO and dEO) in THF solution in a custom heavy-wall glass reaction flask on Schlenk line. Under dry nitrogen atmosphere, either protonated or deuterated BPA dissolved in anhydrous THF at 0 °C, titrated with potassium naphthalene to generate the initiators, followed by addition of hEO or dEO. After stirring for 1 h, the mixture was heated to 50 °C and allowed to react for 3 d. The polymerization was terminated with methanol and the polymer was recovered by precipitation in cold diethyl ether. ^{1}H-nuclear magnetic resonance (^{1}H-NMR: 500 MHz, $CDCl_3$): δ 7.10 ppm (b, 4H), 6.79 ppm (b, 4H), 3.64 ppm (b, 800H), 1.61 ppm (b, 6H). GPC (0.1 M $NaNO_3$ in H_2O): hABAPEG: M_n = 8900 Da, dispersity = 1.26; dABAPEG: M_n = 14 700 Da, dispersity = 1.13.

Phosphorylation of **ABAPEG** was carried out in a flame-dried flask under dry nitrogen atmosphere. At first, **ABAPEG** was dissolved in anhydrous THF at 50 °C, and then phosphorus oxychloride was added at once *via* gas-tight syringe. The solution was stirred under nitrogen pressure for 3 h, followed by the addition of small amount of water for quenching the reaction. After evaporation of THF and dialysis against Milli-Q water, the sample was lyophilized to give a white powder. ^{31}P-NMR (D_2O): δ 0.3 ppm. GPC (0.1 M $NaNO_3$ in H_2O): hPi-ABAPEG: M_n = 10 400 Da, dispersity = 1.20. dPi-ABAPEG: M_n = 17 200 Da, dispersity = 1.15.

DMPC vesicle sample preparation

Both tail-deuterated and fully hydrogenated **DMPC** lipids were purchased from Avanti Polar Lipid. **DMPC** was first dissolved in chloroform with a concentration of 1 mg ml^{-1}. A desired volume of stock solution was then transferred to a glass culture tube with a syringe. Chloroform was removed by blowing with N_2 stream, followed by drying in vacuum with gentle heating (40 °C) for a minimum of 12 h. Dry lipid films were then hydrated with D_2O followed by vigorous vortexing at 40 °C. The resulting multilamellar vesicles suspension was incubated at 40 °C for at least 1 h and then subject to 5 freeze/thaw cycles between −80 °C and 50 °C. ULV were prepared by a handheld miniextruder from Avanti Polar Lipids equipped with a 100 nm pore-diameter polycarbonate filter heated to 40 °C. For each sample, 41 times of the extrusion were performed. Sample concentration after extrusion was 40 mg ml^{-1}, which allows for further mixture with polymer samples to final concentration of 10 mg ml^{-1} for SANS measurements and 20 mg ml^{-1} for NSE measurements.

DLS measurements

Dynamic light Scattering (DLS) was measured at 90° using a BI-200SM goniometer containing a red laser diode with a wavelength of 637 nm and a TurboCorr digital correlator (Brookhaven Instruments, Holtsville, NY). Brookhaven Instruments DLS software was used to analyse the intensity autocorrelation function using the CONTIN method. Before the measurement, hDMPC vesicle solution and hPi-ABAPEG solutions were well mixed to achieve a final polymer mass fraction of 0%, 1% and 3%, and a final vesicle solution of 10 mg ml^{-1}. The samples were kept at 37 °C during the whole period of the measurement.

SANS measurements

SANS data were collected on the NG3-SANS instruments at the Centre for Neutron Research (NCNR) at National Institute of Standards and Technology (NIST)[29] and the CG-3 Bio-SANS

instrument at the High Flux Isotope Reactor (HFIR) at Oak Ridge National Laboratory (ORNL).[30] The incident neutron wavelength, λ, at NIST was selected to be 6 Å for 1 m and 4 m configuration and 8.9 Å for 13 m configuration, with a wavelength resolution of 11%. λ at ORNL was selected to be 6 Å for 1.1 m and 6.8 m configuration and 12 Å for 15.3 m configuration, with a wavelength resolution of 15%. With these configurations, q was measured from 0.001 $Å^{-1}$ to 0.557 $Å^{-1}$ at NIST and from 0.002 $Å^{-1}$ to 0.717 $Å^{-1}$ at ORNL. The sample thickness was 1 mm, loaded in standard quartz banjo cells (Hellma USA, Plainview, NY) and mounted in a temperature-controlled cell holder with 0.1 °C accuracy at NIST and 1 °C at ORNL. The scattered intensity was corrected for instrument dark current, empty cell scattering, the sensitivity of individual detector pixels, and beam transmission to obtain the absolute neutron intensity through the direct beam flux method by use of the available data reduction macros based on the Igor Pro data reduction package provided by NCNR, NIST.[31] The scattering length density (SLD) of pure hPi-ABAPEG and dPi-ABAPEG copolymers were determined from the contrast variation SANS (Fig. S1 and S2, ESI‡). For all conditions, SANS data from the pure dPi-ABAPEG copolymers solution is used as the background for background subtraction. The statistical error bars correspond to one standard deviation. For pure polymer solutions, SANS data was analysed using the worm-like chain model[32] in SASview[33] (Fig. S1, ESI‡).

The SANS data of **DMPC** ULVs was analysed by a core–shell model. We used three shells to describe the tails and heads of **DMPC** bilayer. Two assumptions were made in the fitting: (1) the structures of the inner and outer leaflet of the membrane are decoupled, so any structural change to the outer leaflet of the membrane does not affect the structure of the inner leaflet of the membrane; and (2) the structures of the inner leaflet were assumed to remain intact in all the conditions. Since both tail and head layers are very thin, the condition of $\sigma \ll d$, where σ is interfacial width and d is thickness, is violated. The effective-density model was used to obtain the continuous scattering length density profiles.[34,35] Fittings were simultaneously performed on both protonated **DMPC** (hDMPC) and tail-deuterated **DMPC** (dDMPC) with shared parameters.

NSE measurements

Neutron spin echo measurements were performed at the NCNR on the NGA-NSE spectrometer. Prior to experiments, fresh samples were prepared and then incubated at 37 °C for 3 h, letting the system reach thermal equilibrium. A D_2O and H_2O mixed solvent with a volume ratio of 98.5 : 1.5 was used to reduce the scattering from dPi-ABAPEG copolymers in the q range of NSE measurements. The NSE measurements were conducted at three different q values: λ = 11 Å, q = 0.05 $Å^{-1}$; λ = 8 Å, q = 0.085 $Å^{-1}$; and λ = 8 Å, q = 0.11 $Å^{-1}$. The covered Fourier time was up to 100 ns for λ = 11 Å and 40 ns for λ = 8 Å, respectively. The reduction of NSE data was done using NCNR developed DAVE program[36] and the analysis was performed using NCNR developed Igor macros. The statistical error bars correspond to one standard deviation.

XRR measurements

X-ray reflectivity measurements were all performed at ChemMatCARS sector 15ID-C at the Advanced Photon Source of Argonne National Laboratory. **DMPC** was dissolved in chloroform with a concentration of 1 mg ml^{-1}. 45 μl **DMPC** solution was deposited at the air–water interface at 37 °C, allowed to relax 30 min before compressing to a surface pressure of 20 mN m^{-1}. The reflected intensity as a function of momentum transfer vector $q_z = 4\pi \sin\theta/\lambda$, where θ is the incident angle and λ is the X-ray wavelength. The statistical error bars correspond to one standard deviation. The fitting was done use a previously described procedure.[37,38]

Results and discussion

SANS profiles of **ABAPEG** and **Pi-ABAPEG** copolymers in D_2O with a mass fraction of 1% show no differences at high q range (Fig. S1, ESI‡). Fitting the SANS profiles of two polymers with a worm-like chain model gives almost identical results, suggesting that the polymer chain conformation of **ABAPEG** has no significant changes after end-phosphorylation. Moreover, the deviations of experimental and fitted data at low q values indicate that both of **ABAPEG** and **Pi-ABAPEG** copolymers form aggregates, which give rise to the higher scattering intensity at low q range, and end-phosphorylation of **ABAPEG** leads to larger aggregates.[27] In addition, NSE measurements show that **ABAPEG** and **Pi-ABAPEG** have almost identical chain dynamics in solution at 37 °C (Fig. S3, ESI‡).

End-phosphorylation of **ABAPEG** adding one phosphate group at each end of the polymer does not significantly alter the chain conformation of the polymer in solution. However, it greatly changes the interaction between the polymer and vesicle membranes. We observed that **ABAPEG** induces immediate phase separation of **DMPC** vesicles from solution at a mass fraction of as low as 1%, whereas no phase separation of **DMPC** ULVs was observed for any of the **DMPC** ULV/**Pi-ABAPEG** solution (Fig. 2a). DLS measurements show that, in the presence of up to a mass fraction of 3% **Pi-ABAPEG**, the **DMPC** ULVs are stable up to 60 h at 37 °C, maintaining their hydrodynamic radii except for small changes caused by adding **Pi-ABAPEG** (Fig. 2b). The phase separation of **DMPC** ULVs in the presence of **ABAPEG** is probably induced by an imbalance of osmolality between the depletion layer and bulk aqueous phase of **ABAPEG** in solution.[39,40] The effect of osmotic stress on membrane fusion has been well investigated in a number of different systems using PEG polymers.[41]

The stability of the vesicles in the presence of **Pi-ABAPEG** is further confirmed by SANS measurements on both hDMPC and dDMPC ULVs with a vesicle concentration of 10 mg ml^{-1} at 37 °C. dPi-ABAPEG was used in all the SANS and NSE experiments discussed later. The scattering of these deuterated polymers was further minimized by contrast matching using the mixed solvents of H_2O and D_2O (Fig. S2, ESI‡). Fig. 3a presents the SANS profiles of pure dDMPC ULVs and dDMPC ULVs with mass fractions of 0.5%, 1%, and 2% dPi-ABAPEG in solution. Little changes were

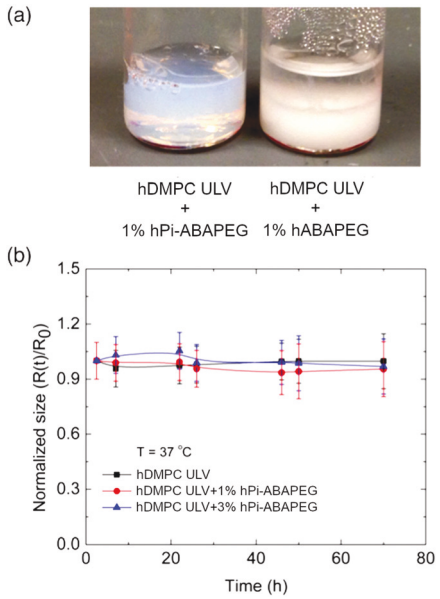

Fig. 2 (a) The hABAPEG causes immediate vesicle phase separation at 37 °C. hPi-ABAPEG does not lead to any vesicle phase separation at 37 °C. (b) DLS measurements show that hDMPC ULV vesicles are stable at 37 °C before and after adding final mass fractions of 1%, and 3% hPi-ABAPEG copolymer. For each condition, the radii measured at different times are normalized by the mean ULV radius measured at time = 0 h from the same condition.

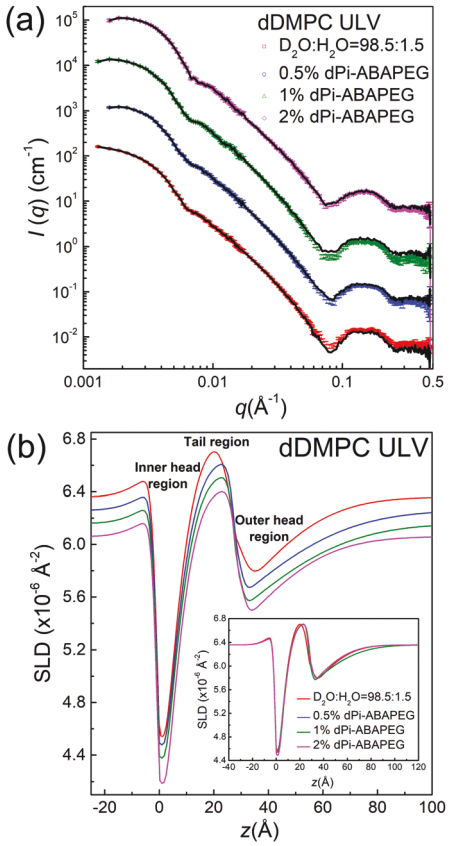

Fig. 3 (a) Measured SANS profiles (symbols) and their corresponding best-fits (black solid lines) of dDMPC ULVs at 37 °C with various mass fractions (0%, 0.5%, 1%, and 2%) of dPi-ABAPEG added into the mixed D_2O/H_2O solution. (b) Scaled SLD profiles extracted from the best-fit results. Both SANS curves and SLD profiles are shifted in the *y*-axis to distinguish different curves. The SLD profiles are shifted and set the inner head surface as zero, so that the SLDs of the inner leaflet are overlapping in order to compare the membrane thicknesses. The inset in (b) show the SLD profiles without shifting in the *y*-axis.

observed in the SANS profiles at the low q range, which mainly contains the size and shape information of vesicles. Similar results were also obtained from ULVs made of hDMPC. However, at the high q regime (0.08 $Å^{-1}$ to 0.2 $Å^{-1}$) of the SANS profiles which mostly contain the information from the lipid membrane, the SANS profiles show some small differences, implying change of membrane structure. This is further confirmed by the best-fitted scattering length density profiles of the dDMPC vesicles (Fig. 3b). In the presence of dPi-ABAPEG, the inner leaf of lipid membrane almost remains intact, whereas the membrane thickness of outer leaf increases about 1–2 Å as the polymer concentration increases from 0% to 2%, as revealed by the slight changes in the SLD profiles. However, this increase of membrane thickness is too small to make more qualitative arguments by this technique alone.

To further investigate the interaction between **Pi-ABAPEG** and **DMPC** membranes, we performed XRR measurements on **DMPC** monolayers at the air–water interface at 37 °C. Fig. 4a shows specular XRR data for **DMPC** monolayers at 20 mN m^{-1} on two subphases (pure water and water with a mass fraction of 0.1% **Pi-ABAPEG**). The XRR spectra show a global shift of the reflectivity to lower values of the wave-vector transfer in the normal direction (z direction), q_z, upon addition of a mass fraction of 0.1% **Pi-ABAPEG** into water, indicating an increase in the thickness of the interface monolayer. Fig. 4b gives the best-fit electron density profiles. The adsorption of **Pi-ABAPEG** increases length of the tail regime in the electron density profile. Assuming the volume of a **DMPC** lipid is a constant, a longer tail means a smaller area per lipid in the lateral direction, which indicates a more compacted **DMPC** monolayer in lateral direction. A close look at the electron density profile also reveals the change of PC head group hydration layer in the presence of **Pi-ABAPEG**. The PC head groups are highly hydrated in water,[41–43] as indicated by a 15 Å regime of elevated electron density near the water–PC head group interface. After the addition of a mass fraction of 0.1% **Pi-ABAPEG**, this regime further extended to 22 Å, evident of the adsorption of **Pi-ABAPEG**.

The chemical structure of **ABAPEG** and **Pi-ABAPEG** are identical except for the two end phosphate groups. The striking differences on the effects of two polymers on the stability of vesicle membranes suggests that the function of PEGylated polymers can be greatly altered by end-chemical modifications. The end-phosphate groups do not introduce any big change in polymer chain conformation (Fig. S1, ESI‡) and dynamics (Fig. S3, ESI‡) in solution. However, the phosphate groups can interact with the PC head groups *via* dipole–ion interaction.[8] The head group of **DMPC** has a dipole. The attractive dipole–ion interaction between a PC head group and a phosphate can lead to polymer adsorption.

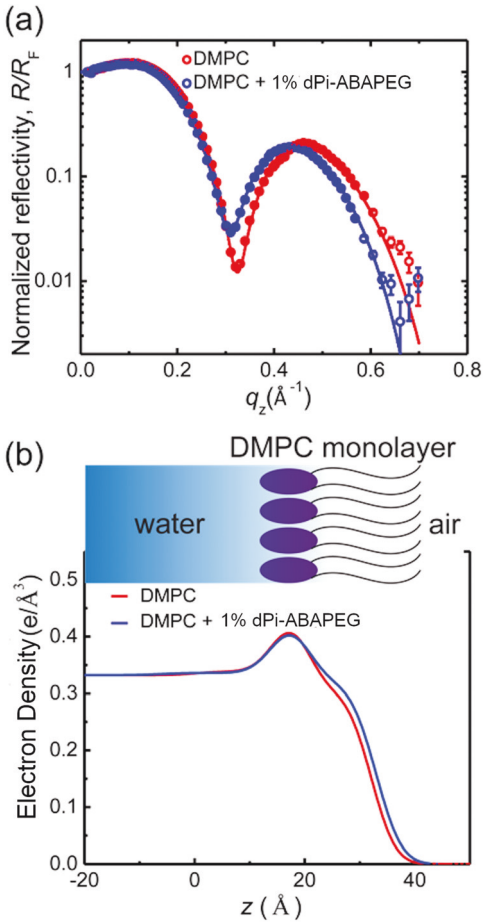

Fig. 4 X-ray reflectivity reveals the adsorption of **Pi-ABAPEG** on a **DMPC** monolayer. (a) Normalized X-ray reflectivity, R/R_F, of **DMPC** monolayers at the air–water interface and water with a mass fraction of 0.1% dPi-ABAPEG subphases. R_F stands for Fresnel reflectivity. (b) Electron density profiles of **DMPC** monolayers on water and water with a mass fraction of 0.1% dPi-ABAPEG subphases. The interface of water and lipid head region is set as zero and the electron density profiles are shifted for comparison. The adsorption of dPi-ABAPEG changes the electron density of the water layer near the PC head groups, indicating that the polymer interrupts the hydration layer of PC head groups.

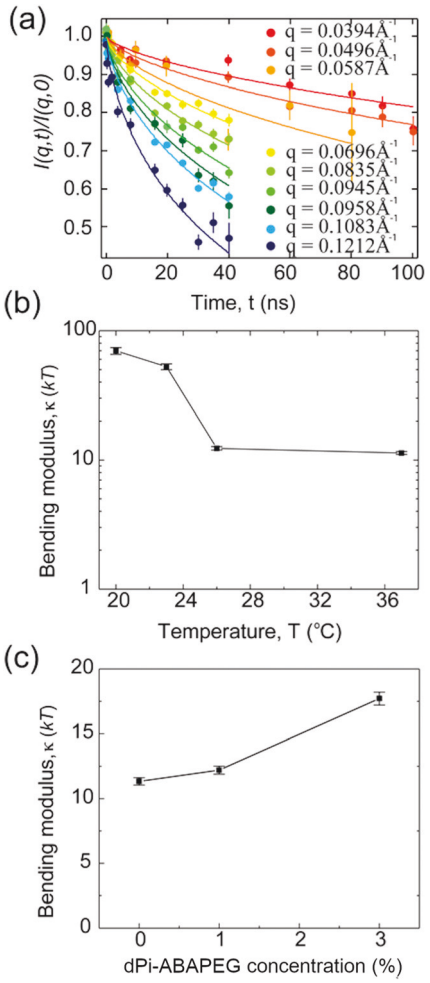

Fig. 5 (a) $I(q,t)/I(q,0)$ of **DMPC** vesicles at T = 37 °C are fit to eqn (1). (b) Temperature dependence of κ. (c) dPi-ABAPEG concentration dependence of κ. The bending modulus, κ, of **DMPC** vesicle membrane increases with polymer concentrations.

To explore the interaction of **Pi-ABAPEG** on **DMPC** membranes further, NSE measurements were performed to examine the dynamics of polymer-induced shape fluctuations of **DMPC** ULVs. The normalized intermediate dynamic structure factor $I(q,t)/I(q,0)$ of the **DMPC** ULV in dPi-ABAPEG D_2O/H_2O (98.5/1.5 v/v)-mixed solution at different dPi-ABAPEG concentration were measured at 37 °C using NSE (Fig. 5a).

The modified Zilman and Granek model describes the intermediate dynamics structure factor of a membrane at a q region that is sensitive to single membrane dynamics.[11,44–46] At sufficiently large q ($qR \gg 1$ where R is the radius of the ULV), the intermediate dynamics structure factor of a thermally fluctuating bilayer membrane can be expressed by the following equations:

$$\frac{I(q,t)}{I(q,0)} = \exp\left[-(\Gamma(q)t)^{\frac{2}{3}}\right], \quad (1)$$

and $\Gamma(q)$ is given by

$$\Gamma(q) = 0.025\alpha\left(\frac{k_B T}{\tilde{\kappa}}\right)^{1/2}\frac{k_B T}{\eta_{D_2O}}q^3, \quad (2)$$

where α is a parameter close to unity for large κ originating from averaging the angle between the wave vectors and a vector normal to the bilayer structure, η_{D_2O} is the viscosity of D_2O, k_B is the Boltzmann's constant, and $\tilde{\kappa}$ is the effective bending modulus including the interlayer friction $\tilde{\kappa}$ can be expressed by $\tilde{\kappa} = \kappa + 2d^2k_m$, where d is the height of the neutral surface from the bilayer midplane, k_m is the monolayer lateral compressibility modulus, and is κ the intrinsic bending modulus.[43] Since the radius of the **DMPC** ULV used in this study is around 500 Å, the requirement of $qR \gg 1$ is satisfied for the q range measured in this study. The relatively small size and the distribution of the size of the **DMPC** ULV scan affect the membrane bending modulus, as the membrane bending rigidity may increase with decreasing size for small size vesicles.[47] The osmotic pressure of the **Pi-ABAPEG** copolymer in solution can also impact the elasticity of **DMPC**

membranes,[40] and may cause lateral inhomogeneity of the **DMPC** bilayer associated with the polymer.[48,49] An advantage of the NSE technique is that it measures ensemble average of the membrane dynamics, so it can provide the average values of membrane bending rigidity for our system.[11,45]

We first studied the temperature dependence of the bending modulus, κ, of pure **DMPC** ULVs. As expected, κ increases with decreasing temperature, and a clear transition across the phase transition temperature, T_m, of **DMPC** around 24 °C is measured (Fig. 5b). The values of κ measured at different temperatures within the uncertainty of our measurements are in agreement with the values reported in the literature.[8,46,50–53] To study the effect of dPi-ABAPEG to the membrane dynamics, the bending moduli κ of **DMPC** ULV were then measured with mass fractions of 1%, and 3% dPi-ABAPEG added in a D_2O/H_2O (98.5/1.5 v/v)-mixed solvent. κ increases from (11.3 ± 0.3) kT to (17.7 ± 0.5) kT with dPi-ABAPEG concentration (Fig. 5c). This increase of membrane rigidity can be partially caused by the bilayer thickening as suggested by the XRR results. The adsorption of dPi-ABAPEG and the osmotic pressure of the polymer in solution can also cause a more laterally compacted bilayer, and thus can affect the elasticity of **DMPC** membrane.[25,27,47,48] The good agreement between our XRR and NSE bending rigidity results strongly support our hypothesis that the adsorption of dPi-ABAPEG strongly impacts the dynamics and elasticity of the membrane. Our results are consistent with previous studies, which have shown that the protective effects of the dPi-ABAPEG copolymer and some other PEGylated polymers root from the polymer adsorption at the membrane surface without penetrating into the bilayer.[4,25,27] The adsorbed polymer effectively retards membrane hydration dynamics, and thereby, exerts its membrane sealing function.[25]

Conclusions

In summary, end phosphorylation of **ABAPEG** changes the interaction between the PEG polymer and **DMPC** membranes significantly. The structure, thermal fluctuation and elasticity of **DMPC** ULV membranes interacting with **Pi-ABAPEG**, have been investigated by XRR, SANS and NSE measurements. The adsorption of **Pi-ABAPEG** does not significantly change the membrane structure, but increases the membrane bending modulus, κ. Our results highlight the importance of end functional groups of PEGylated polymers to the functionality of the polymer. The information obtained by NSE allows us to gain critical insights on membrane dynamics in the presence of extracellular macromolecules.

Conflicts of interest

There are no conflicts to declare.

Acknowledgements

Work in the Centre for Molecular Engineering and Materials Science Division of Argonne National Laboratory was supported by the U.S. Department of Energy, Office of Science, Office of Basic Energy Sciences, Materials Science and Engineering Division. M. N. and Y. L. acknowledge funding support of cooperative agreement 70NANB15H259 and 70NANB15H260, respectively, from NIST, U.S. Department of Commerce. Access to the NG3-SANS instrument and NGA-NSE spectrometer was provided by the Center for High Resolution Neutron Scattering, a partnership between NIST and the NSF under Agreement No. DMR-1508249. NSF's ChemMatCARS Sector 15 is supported by the Divisions of Chemistry (CHE) and Materials Research (DMR), National Science Foundation, under grant number NSF/CHE-1834750. This research used resources of the Advanced Photon Source (APS) and the Centre for Nanoscale Materials (CNM), a U.S. Department of Energy (DOE) Office of Science User Facility operated for the DOE Office of Science by Argonne National Laboratory under Contract No. DE-AC02-06CH11357. A portion of the synthesis was conducted at the Centre for Nanophase Materials Sciences (CNMS), which is the DOE Office of Science User Facilities. Part of the SANS was done on the CG-3 Bio-SANS instrument at the High Flux Isotope Reactor (HFIR), which is sponsored by the Office of Biological & Environmental Research in the Department of Energy's Office of Science. This work benefited from the use of the SasView application, originally developed under NSF award DMR-0520547. SasView contains code developed with funding from the European Union's Horizon 2020 Research and Innovation Programme under the SINE2020 project, grant agreement no. 654000. In addition, we gratefully acknowledge the computing resources provided on Bebop, a high-performance computing cluster operated by the Laboratory Computing Resource Centre at Argonne National Laboratory.

Notes and references

1 D. Bhadra, S. Bhadra, P. Jain and N. K. Jain, *Pharmazie*, 2002, **57**, 5.
2 World Intellectual Property Organization, WO2018064536A1, 2018.
3 J. Mao, A. Zaborin, V. Poroyko, D. Goldfeld, N. A. Lynd, W. Chen, M. V. Tirrell, O. Zaborina and J. C. Alverdy, *ACS Biomater. Sci. Eng.*, 2017, **3**, 2076.
4 A. Zaborin, J. R. Defazio, M. Kade, B. L. D. Kaiser, N. Belogortseva, D. G. Camp, R. D. Smith, J. N. Adkins, S. M. Kim, A. Alverdy, D. Goldfeld, M. A. Firestone, J. H. Collier, B. Jabri, M. Tirrell, O. Zaborina and J. C. Alverdy, *Antimicrob. Agents Chemother.*, 2014, **58**, 966.
5 V. Valuckaite, O. Zaborina, J. Long, M. Hauer-Jensen, J. R. Wang, C. Holbrook, A. Zaborin, K. Drabik, M. Katdare, H. Mauceri, R. Weichselbaum, M. A. Firestone, K. Y. Lee, E. B. Chang, J. Matthews and J. C. Alverdy, *Am. J. Physiol.: Gastrointest. Liver Physiol.*, 2009, **297**, 1041.
6 L. T. Boni, T. P. Stewart, J. L. Alderfer and S. W. Hui, *J. Membr. Biol.*, 1981, **62**, 71.
7 T. L. Kuhl, J. Majewski, P. B. Howes, K. Kjaer, A. von Nahmen, K. Y. C. Lee, B. Ocko, J. N. Israelachvili and G. S. Smith, *J. Am. Chem. Soc.*, 1999, **121**, 7682.

8 J. N. Israelachvili, *Intermolecular and surface forces*, Academic Press, Burlington, MA, 3rd edn, 2011.
9 A. J. Garcia-Saez, S. Chiantia and P. Schwille, *J. Biol. Chem.*, 2007, **282**, 33537.
10 J. Pan, S. Tristram-Nagle, N. Kucerka and J. F. Nagle, *Biophys. J.*, 2008, **94**, 117.
11 A. C. Woodka, P. D. Butler, L. Porcar, B. Farago and M. Nagao, *Phys. Rev. Lett.*, 2012, **109**, 058102.
12 J. Henriksen, A. C. Rowat and J. H. Ipsen, *Eur. Biophys. J.*, 2004, **33**, 732.
13 R. Dimova, *Adv. Colloid Interface Sci.*, 2014, **208**, 225.
14 J. Henriksen, A. C. Rowat, E. Brief, Y. W. Hsueh, J. L. Thewalt, M. J. Zuckermann and J. H. Ipsen, *Biophys. J.*, 2006, **90**, 1639.
15 M. Kummrow and W. Helfrich, *Phys. Rev. A: At., Mol., Opt. Phys.*, 1991, **44**, 8356.
16 Y. Takechi-Haraya, K. Sakai-Kato, Y. Abe, T. Kawanishi, H. Okuda and Y. Goda, *Langmuir*, 2016, **32**, 6074.
17 R. Dimova, K. Danov, B. Pouligny and I. B. Ivanov, *J. Colloid Interface Sci.*, 2000, **226**, 35.
18 N. Kucerka, S. Tristram-Nagle and J. F. Nagle, *J. Membr. Biol.*, 2005, **208**, 193.
19 Y. Lyatskaya, Y. F. Liu, S. Tristram-Nagle, J. Katsaras and J. F. Nagle, *Phys. Rev. E*, 2001, **63**, 011907.
20 Z. Yi, M. Nagao and D. P. Bossev, *J. Phys.: Condens. Matter*, 2009, **21**, 155104.
21 D. M. Engelman, *Nature*, 2005, **438**, 578.
22 H. Lee and R. W. Pastor, *J. Phys. Chem. B*, 2011, **115**, 7830.
23 J. H. Lee, S. M. Doe, C. Choi, A. Faraone, P. A. Pincus and S. R. Kline, *Phys. Rev. Lett.*, 2010, **105**, 038101.
24 D. Marguet, P. F. Lenne, H. Rigneault and H. T. He, *EMBO J.*, 2006, **25**, 3446.
25 C. Y. Cheng, J. Y. Wang, R. Kausik, K. Y. C. Lee and S. Han, *Biomacromolecules*, 2012, **13**, 2624.
26 Z. A. Levine, R. M. Venable, M. C. Watson, M. G. Lerner, J. E. Shea, R. W. Pastor and F. L. H. Brown, *J. Am. Chem. Soc.*, 2014, **136**, 13582.
27 J. Y. Wang, J. Marks and K. Y. C. Lee, *Biomacromolecules*, 2012, **13**, 2616.
28 J. E. Nielsen, V. A. Bjørnestad and R. Lund, *Soft Matter*, 2018, **14**, 8750–8763.
29 S. M. Choi, J. G. Barker, C. J. Glinka, Y. T. Cheng and P. L. Gammel, *J. Appl. Crystallogr.*, 2000, **33**, 793.
30 G. W. Lynn, W. Heller, V. Urban, G. D. Wignall, K. Weiss and D. A. A. Myles, *Phys. B*, 2006, **385–386**, 880.
31 S. R. Kline, *J. Appl. Crystallogr.*, 2006, **39**, 895–900.
32 J. S. Pedersen and P. Schurtenberger, *Macromolecules*, 1996, **29**, 7602.
33 http://www.sasview.org/.
34 M. Tolan, *X-ray scattering from soft-matter thin films: materials science and basic research*, Springer, New York, 1999.
35 Z. Jiang and W. Chen, *J. Appl. Crystallogr.*, 2017, **50**, 1653–1663.
36 R. T. Azuah, L. R. Kneller, Y. M. Qiu, P. L. W. Tregenna-Piggott, C. M. Brown, J. R. D. Copley and R. M. Dimeo, *J. Res. Natl. Inst. Stand. Technol.*, 2009, **114**, 341.
37 W. Bu, M. Mihaylov, D. Amoanu, B. H. Lin, M. Meron, I. Kuzmenko, L. Soderholm and M. L. Schlossman, *J. Phys. Chem. B*, 2014, **118**, 12486.
38 W. Bu, D. Vaknin and A. Travesset, *Langmuir*, 2006, **22**, 5673.
39 B. R. Lentz, *Chem. Phys. Lipids*, 1994, **73**, 91.
40 V. S. Malinin, P. Frederik and B. R. Lentz, *Biophys. J.*, 2002, **82**, 2090.
41 J. N. Israelachvili and H. Wennerstrom, *Langmuir*, 1990, **6**, 873.
42 R. P. Rand and V. A. Parsegian, *Annu. Rev. Physiol.*, 1986, **48**, 201.
43 A. G. Zilman and R. Granek, *Phys. Rev. Lett.*, 1996, **77**, 4788.
44 M. C. Watson and F. L. H. Brown, *Biophys. J.*, 2010, **98**, L9.
45 A. G. Zilman and R. Granek, *Chem. Phys.*, 2002, **284**, 195.
46 M. Nagao, E. G. Kelley, R. Ashkar, R. Bradbury and P. D. Butler, *J. Phys. Chem. Lett.*, 2017, **8**, 4679.
47 J. A. Jackman, G. H. Zan, V. P. Zhdanov and N. J. Cho, *J. Phys. Chem. B*, 2013, **117**, 16117.
48 T. Hamada, Y. Kishimoto, T. Nagasaki and M. Takagi, *Soft Matter*, 2011, **7**, 9061.
49 K. Oglecka, P. Rangamani, B. Liedberg, R. S. Kraut and A. N. Parikh, *eLife*, 2014, **3**, e03695.
50 W. T. Heller and P. A. Zolnierczuk, *Biochim. Biophys. Acta, Biomembr.*, 2019, **1861**, 565.
51 R. Sreij, C. Dargel, P. Geisler, Y. Hertle, A. Radulescu, S. Pasini, J. Perez, L. H. Moleiro and T. Hellweg, *Phys. Chem. Chem. Phys.*, 2018, **20**, 9070.
52 V. K. Sharma, M. Nagao, D. K. Rai and E. Mamontov, *Phys. Chem. Chem. Phys.*, 2019, **21**, 20211.
53 J.-Y. Wang, W. Chen, M. Nagao, P. Shelat, B. A. G. Hammer, G. T. Tietjen, K. D. Cao, J. M. Henderson, L. He, B. Lin, B. Akgun, M. Meron, S. Qian, S. Ward, J. D. Marks, T. Emrick and K. Y. C. Lee, *Biomacromolecules*, 2019, **20**, 3385.